


RESEARCH

Open Access



Comparison of manual and artificial intelligence-automated choroidal thickness segmentation of optical coherence tomography imaging in myopic adults

Zhi Wei Lim¹, Jonathan Li², Damon Wong^{3,4,5,6}, Joey Chung³, Angeline Toh³, Jia Ling Lee³, Crystal Lam³, Maithily Balakrishnan³, Audrey Chia^{3,7}, Jacqueline Chua^{3,4,5}, Michael Girard^{3,7,8}, Quan V. Hoang^{10,3,7,9}, Rachel Chong^{3,7}, Chee Wai Wong³, Seang Mei Saw^{11,3,7}, Leopold Schmetterer^{12,13,3,5,6,7,8}, Noel Brennan¹⁴ and Marcus Ang^{3,4*} 

Abstract

Background Myopia affects 1.4 billion individuals worldwide. Notably, there is increasing evidence that choroidal thickness plays an important role in myopia and risk of developing myopia-related conditions. With the advancements in artificial intelligence (AI), choroidal thickness segmentation can now be automated, offering inherent advantages such as better repeatability, reduced grader variability, and less reliance for manpower. Hence, we aimed to evaluate the agreement between AI-automated and manual segmented measurements of subfoveal choroidal thickness (SFCT) using two swept-source optical coherence tomography (OCT) systems.

Methods Subjects aged ≥ 16 years, with myopia of ≥ 0.50 diopters in both eyes, were recruited from the Prospective Myopia Cohort Study in Singapore (PROMYSE). OCT scans were acquired using Triton DRI-OCT and PLEX Elite 9000. OCT images were segmented both automatically with an established SA-Net architecture and manually using a standard technique with adjudication by two independent graders. SFCT was subsequently determined based on the segmentation. The Bland–Altman plot and intraclass correlation coefficient (ICC) were used to evaluate the agreement.

Results A total of 229 subjects (456 eyes) with mean [\pm standard deviation (SD)] age of 34.1 (10.4) years were included. The overall SFCT (mean \pm SD) based on manual segmentation was $216.9 \pm 82.7 \mu\text{m}$ with Triton DRI-OCT and $239.3 \pm 84.3 \mu\text{m}$ with PLEX Elite 9000. ICC values demonstrated excellent agreement between AI-automated and manual segmented SFCT measurements (PLEX Elite 9000: ICC = 0.937, 95% CI: 0.922 to 0.949, $P < 0.001$; Triton DRI-OCT: ICC = 0.887, 95% CI: 0.608 to 0.950, $P < 0.001$). For PLEX Elite 9000, manual segmented measurements were generally thicker when compared to AI-automated segmented measurements, with a fixed bias of $6.3 \mu\text{m}$ (95% CI: 3.8 to 8.9, $P < 0.001$) and proportional bias of 0.120 ($P < 0.001$). On the other hand, manual segmented measurements were comparatively thinner than AI-automated segmented measurements for Triton DRI-OCT, with a fixed bias of $-26.7 \mu\text{m}$ (95% CI: -29.7 to -23.7 , $P < 0.001$) and proportional bias of -0.090 ($P < 0.001$).

*Correspondence:

Marcus Ang

marcus.ang@SNEC.com.sg

Full list of author information is available at the end of the article



© The Author(s) 2024. **Open Access** This article is licensed under a Creative Commons Attribution 4.0 International License, which permits use, sharing, adaptation, distribution and reproduction in any medium or format, as long as you give appropriate credit to the original author(s) and the source, provide a link to the Creative Commons licence, and indicate if changes were made. The images or other third party material in this article are included in the article's Creative Commons licence, unless indicated otherwise in a credit line to the material. If material is not included in the article's Creative Commons licence and your intended use is not permitted by statutory regulation or exceeds the permitted use, you will need to obtain permission directly from the copyright holder. To view a copy of this licence, visit <http://creativecommons.org/licenses/by/4.0/>. The Creative Commons Public Domain Dedication waiver (<http://creativecommons.org/publicdomain/zero/1.0/>) applies to the data made available in this article, unless otherwise stated in a credit line to the data.

Conclusion We observed an excellent agreement in choroidal segmentation measurements when comparing manual with AI-automated techniques, using images from two SS-OCT systems. Given its edge over manual segmentation, automated segmentation may potentially emerge as the primary method of choroidal thickness measurement in the future.

Keywords Choroidal thickness, Myopia, Optical coherence tomography, Automated segmentation, Manual segmentation

Background

Globally, myopia affects 1.4 billion individuals, amounting to 23% of the world population [1]. Those suffering from high myopia (163 million individuals) are exposed to an increased risk of pathologic myopia and subsequent visual impairment [2, 3]. There is now increasing evidence that the choroid plays an important role in myopia and risk of developing pathology related to myopia [4–9]. Thinner choroids have been observed to be significantly associated with longer axial lengths, myopic spherical equivalent and more importantly, an increased risk of poorer best corrected visual acuity and myopic macular degeneration (MMD) [4–14]. Given its clinical significance, choroidal thickness has been employed as a biomarker for the staging of MMD [15].

Recently, imaging of the choroid has improved with newer optical coherence tomography (OCT) technologies, including the enhanced depth imaging spectral-domain OCT (EDI SD-OCT) and swept-source OCT (SS-OCT) [16, 17]. The SS-OCT utilizes a novel tuneable laser with increased operating wavelength that is capable of deeper tissue penetration with reduced light scattering and faster image acquisition, enabling enhanced tomography of the choroid [18, 19]. Given the vast array of imaging protocols and segmentation algorithms adopted across manufacturers, it is essential to determine the agreement between OCT machines, as this would facilitate clinical interpretation and comparison between inter-modality measurements [18, 20–27]. To the best of our knowledge, there have been no studies comparing choroidal thickness measurements between two established swept-source OCT modalities – Triton DRI-OCT and PLEX Elite 9000.

Furthermore, with the advancements in artificial intelligence (AI), choroidal thickness segmentation can now be automated [28–31]. As compared with manual segmentation, AI-automated segmentation possesses the intrinsic advantages of better repeatability with reduced inter- and intra-grader variability, and the need for less manpower. With these attributes, clinicians using AI-automated segmentation can be more certain of the significance of inter-visit changes detected in choroidal thickness and measurements may be more feasible to perform in day-to-day clinical setting. In this regard, Cahyo et al.

recently introduced a novel multi-task learning approach – SA-Net, aimed to perform automated choroidal segmentation of 3-dimensional (3D) OCT images in the clinical setting [28]. Nonetheless, automated measurements derived using SA-Net have yet to be compared to manually segmented choroidal measurements.

Hence, the objective of our study is to evaluate the choroidal thickness in a population of myopic adults and ascertain the agreement in choroidal thickness measurements using a previously described AI-automated (SA-Net) technique versus a manual segmentation technique, in two different SS-OCT systems. In addition, we aim to evaluate the agreement in choroidal thickness between both SS-OCT modalities as a secondary objective of the study. Findings from this study will contribute towards utilizing choroidal thickness as a clinical biomarker in myopia and establishing meaningful comparisons between choroidal thickness measured with different OCT modalities.

Methods

Study population

We conducted a cross-sectional study utilizing subjects recruited from the ongoing Prospective Myopia Cohort Study in Singapore (PROMYSE). In brief, subjects aged 16 years and over, with myopia of ≥ 0.50 diopters in both eyes, were recruited from the Singapore National Eye Centre (SNEC) from July 2019 to May 2022. For this study, we included subjects with OCT assessments from both Triton DRI-OCT and PLEX Elite 9000. Subjects with poor OCT scan quality or ocular diseases which may impede the accuracy of OCT acquisition, such as significant corneal opacities, advanced cataracts, vitreous opacities, retinal detachment, retinal dystrophies, macular oedema, and macular scarring, were excluded. All study procedures adhered to the principles of the Declaration of Helsinki. Ethics approval was obtained from the Centralized Institutional Review Board of Singapore Health Services (CIRB Reference Number: 2019/2069). Written informed consent was obtained from all subjects.

Ophthalmic assessment

All subjects underwent comprehensive ophthalmic examinations at SNEC. Presenting visual acuity was measured

using the logarithm of the minimum angle of resolution (LogMAR) chart (Lighthouse International, New York, NY, USA). Manifest refraction was subsequently performed by certified research optometrists and spherical equivalent was determined as the sum of spherical power and half of cylindrical power. Anterior and posterior segment examinations were performed by ophthalmologists using slit lamp biomicroscopy after pupillary dilation as specified below. Axial length was measured using IOL Master (Carl Zeiss Meditec, AG, Jena, Germany). An axial length of ≥ 26 mm was defined as high myopia [32]. Fundus photographs and SS-OCT scans were acquired following pupillary dilation with the administration of two drops of tropicamide 1%, five minutes apart. Myopia-related retinal morphological changes were documented, namely peripapillary atrophy (PPA), disc tilt, MMD and MMD-plus [based on the meta-analyses of pathologic myopia study (META-PM)] [33], macular hole, myopic tractional maculopathy (MTM), peripheral retinal degeneration, retinoschisis, posterior staphyloma, epiretinal membrane (ERM), dome shaped macula (DSM), and intrachoroidal cavitation. MMD consisted of five categories – no myopic retinal degenerative lesion (category 0), tessellated fundus (category 1), diffuse chorioretinal atrophy (category 2), patchy chorioretinal atrophy (category 3), and macular atrophy (category 4). MMD-plus was defined as the presence of plus lesions – lacquer cracks, myopic choroidal neovascularization, and Fuchs spot [33].

Measurement of choroidal thickness

Choroidal thickness measurements were obtained using Triton DRI-OCT (Topcon Medical Systems, Oakland, NJ, USA) and PLEX Elite 9000 (Carl Zeiss Meditec, Dublin, CA, USA). SS-OCT scans by both modalities were acquired within the same clinical visit to reduce unwanted effects of diurnal variation on choroidal thickness [34]. Notably, the Triton DRI-OCT uses a swept-source laser with an operational wavelength of 1050 nm and scanning speed of 100,000 A-scans per second. It has an axial and transverse resolution of 8 μm and 20 μm , respectively [35]. Similarly, the PLEX Elite 9000 utilizes a swept-source tuneable laser with an operational wavelength of 1040–1060 nm and scanning speed of 100,000 A-scans per second. It has a comparable axial and transverse resolution of 6.3 μm and 20 μm , respectively [36].

For Triton DRI-OCT, we employed the 3D Macula+Line (horizontal) scan protocol for image acquisition. The 3D macula imaging protocol scans an area of 7.0 \times 7.0 mm with a resolution of 512 \times 256, while the Line imaging protocol scans a length of 9.0 mm with a resolution of 1024 [35]. On the other hand, for PLEX Elite 9000, we employed the AngioPLEX™ protocol which scans an

area of 3.0 \times 3.0 mm [36]. For both OCT modalities, we performed manual and automated segmentation for choroidal thickness measurements.

For manual segmentation, we utilized the default lines plotted by the manufacturer's proprietary software and subsequently manually adjusted them, if necessary. Segmentation lines were plotted at the Bruch's membrane and choroidal–scleral interface. Measurement callipers were subsequently used to manually measure the distance between both segmentation lines subfoveally. To reduce inter-grader variability, choroidal thickness measurements were conducted independently by two trained graders. We masked the graders from the subject's demographic data and ocular parameters to prevent intra-grader bias. Measurements from both graders were subsequently compared. If the inter-grader difference exceeded 10%, both graders collaboratively reviewed the image with a third adjudicator if necessary (Supplementary Fig. 1). Early Treatment Diabetic Retinopathy Study (ETDRS) grid choroidal thickness values derived from Triton's proprietary software were also documented for Triton OCT images [37].

For automated segmentation, we utilized a previously described multi-task learning architecture – SA-Net (Fig. 1) [28]. In brief, this architecture comprises two branches, for reconstruction and segmentation. During reconstruction, the spatial context from adjacent cross-sectional slices are aggregated to form a central slice. Spatial context acquired is subsequently fused with a U-Net based architecture for segmentation. A five-fold cross-validation approach was adopted to train and assess the algorithm using a high myopia dataset [28]. Stratified sampling was performed over the choroidal volume for each fold to ensure that a similar distribution was achieved and to avoid dataset bias. To further avoid training bias and

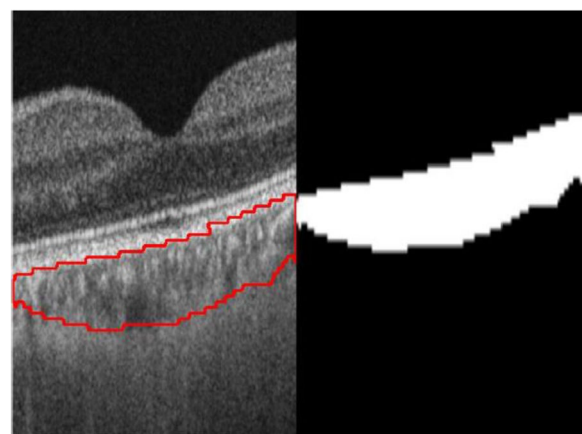


Fig. 1 Automated segmentation by SA-Net

risk of overfitting, all images from the same eye were in the same fold. Further details can be found in the prior work [28]. Choroidal thickness measurements were then derived automatically based on the difference between the upper and lower bounds of the choroid. AI-automated segmentation was performed for both PLEX Elite 9000 and Triton DRI-OCT images, and each was compared to its own manual measurements.

Statistical analysis

All statistical analyses were performed using SPSS statistical software (version 28; IBM, Chicago, IL, USA). Descriptive characteristics were calculated for those who met the inclusion criteria. Independent t-test and Chi-squared/ Fisher's exact test were performed for continuous variables and categorical variables, respectively, to compare subject characteristics between different age groups (<40 years versus \geq 40 years) and axial length (<26.0 mm versus \geq 26.0 mm). Choroidal thickness (measured by Triton DRI-OCT) was further stratified into ETDRS grid areas. Multivariable linear regression analysis was also performed to evaluate the association between age, gender, and axial length with choroidal thickness across the different ETDRS grid areas. Linear mixed models were used to account for inter-eye correlation.

The Bland–Altman plot was used to illustrate the agreement between automated and manual segmented choroidal thickness measurements, in which the difference between choroidal thickness measurements (manual segmented measurements minus automated segmented measurements) was plotted against the mean value [38]. Proportion of outliers was determined by dividing the number of datapoints beyond the 95% limits of agreement (LOA) by the total number of measurements. Additionally, the one-sample t-test and linear regression model were performed to evaluate the presence of fixed and proportional bias, respectively. Intraclass correlation coefficient (ICC) was calculated based on a two-way mixed effects absolute agreement model to further assess the magnitude of agreement [39]. Pearson correlation coefficient was used to evaluate the correlation between automated and manual segmented choroidal thickness measurements. Correlation and agreement analyses were further stratified by axial length (<26.0 mm versus \geq 26.0 mm) and choroidal thickness (<300 μ m versus \geq 300 μ m). Similar analyses were performed to evaluate the agreement and correlation between choroidal thickness measurements from PLEX Elite 9000 and Triton DRI-OCT.

Results

Two hundred and thirty-two subjects (464 eyes) underwent both Triton DRI-OCT and PLEX Elite 9000 scans. Eight eyes were excluded due to poor OCT scan quality. Consequently, 456 eyes from 229 subjects were included for analysis.

Table 1 details the demographics and ocular characteristics of the study subjects. The mean \pm standard deviation (SD) age and visual acuity for subjects included for analysis were 34.1 ± 10.4 years and 0.02 ± 0.03 LogMAR, respectively. The mean \pm SD subfoveal choroidal thickness based on manual segmentation was 216.9 ± 82.7 μ m with Triton DRI-OCT and 239.3 ± 84.3 μ m with PLEX Elite 9000. Those aged \geq 40 years had significantly poorer visual acuity, less myopic spherical equivalent, thinner choroid, higher grade of PPA, higher grade of MMD, and higher prevalence of retinoschisis, posterior staphyloma, ERM, DSM, and intrachoroidal cavitation; they had a lower prevalence of peripheral retinal degeneration (all $P \leq 0.049$). Subjects with axial length \geq 26 mm were more likely to be male, had poorer visual acuity, higher myopic spherical equivalent, thinner choroid, higher grade of PPA, disc tilt, and MMD, as well as a higher prevalence of posterior staphyloma and DSM (all $P \leq 0.045$).

Table 2 details the agreement and correlation between manual and automated segmented choroidal thickness measurements for Triton DRI-OCT and PLEX Elite 9000. Both modalities demonstrated excellent agreement (PLEX Elite 9000: ICC=0.937, 95% CI: 0.922 to 0.949, $P < 0.001$; Triton DRI-OCT: ICC=0.887, 95% CI: 0.608 to 0.950, $P < 0.001$) and correlation (PLEX Elite 9000: $r=0.946$, $P < 0.001$; Triton DRI-OCT: $r=0.933$, $P < 0.001$) between manual and automated segmented choroidal thickness measurements. For PLEX Elite 9000, manual segmented measurements were generally thicker as compared with automated segmented measurements, with a fixed bias of 6.344 μ m (95% CI: 3.802 to 8.886, $P < 0.001$, 95% LOA = -47.787 to 60.475; Fig. 2a) and proportional bias of 0.120 ($P < 0.001$). On the contrary, Triton DRI-OCT manual segmented measurements were comparatively thinner than automated segmented measurements, with a fixed bias of -26.714 μ m (95% CI: -29.711 to -23.716 , $P < 0.001$, 95% LOA = -90.556 to 37.127; Fig. 3a) and proportional bias of -0.090 ($P < 0.001$). Agreement and correlation between manual and automated segmented choroidal thickness remained excellent following stratification for axial length (<26 mm versus \geq 26 mm; Figs. 2b, 2c, 3b, and 3c). On the other hand, following stratification for choroidal thickness, subjects with choroidal thickness \geq 300 μ m demonstrated weaker agreement and correlation with a larger magnitude of fixed bias when compared with those with choroidal thickness <300 μ m (Figs. 2d, 2e, 3d, and 3e).

Table 1 Comparison of baseline characteristics between subjects stratified by age and axial length

| Demographics | Age < 40 years (N = 154) | Age ≥ 40 years (N = 75) | P value [†] | Axial length < 26 mm (N = 96) | Axial length ≥ 26 mm (N = 133) | P value [†] | Total (N = 229) |
|---|--|-------------------------------------|----------------------------|--|---|----------------------------|----------------------------|
| Age (years) | 28.1 ± 6.2 | 46.5 ± 4.5 | < 0.001 | 34.0 ± 10.5 | 34.2 ± 10.4 | 0.926 | 34.1 ± 10.4 |
| Gender (male; n) | 73 (47.4%) | 28 (37.3%) | 0.150 | 33 (34.4%) | 68 (51.1%) | 0.012 | 101 (44.1%) |
| Ethnicity (n) | | | | | | | |
| • Chinese | 147 (95.5%) | 73 (97.3%) | 1.000 | 91 (94.8%) | 129 (97.0%) | 0.760 | 220 (96.1%) |
| • Malay | 3 (1.9%) | 1 (1.3%) | | 2 (2.1%) | 2 (1.5%) | | 4 (1.7%) |
| • Indian | 4 (2.6%) | 1 (1.3%) | | 3 (3.1%) | 2 (1.5%) | | 5 (2.2%) |
| Ocular characteristics | Age < 40 years (n = 308) | Age ≥ 40 years (n = 148) | P value[†] | Axial length < 26 mm (n = 188) | Axial length ≥ 26 mm (n = 268) | P value[†] | Total (n = 456) |
| Ocular parameters | | | | | | | |
| Visual acuity (LogMAR) | 0.02 ± 0.02 | 0.03 ± 0.05 | 0.021 | 0.01 ± 0.02 | 0.03 ± 0.04 | < 0.001 | 0.02 ± 0.03 |
| Axial length (mm) | 26.4 ± 1.4 | 26.4 ± 1.4 | 0.992 | 25.1 ± 0.6 | 27.3 ± 1.1 | < 0.001 | 26.4 ± 1.4 |
| Spherical equivalent (D) | -6.2 ± 2.9 | -5.4 ± 3.8 | 0.015 | -4.4 ± 1.7 | -7.0 ± 3.6 | < 0.001 | -5.9 ± 3.3 |
| Choroidal thickness (µm) | | | | | | | |
| • Triton DRI-OCT | 222.5 ± 79.9 | 205.3 ± 87.2 | 0.038 | 255.3 ± 82.0 | 190.1 ± 71.9 | < 0.001 | 216.9 ± 82.7 |
| • PLEX Elite 9000 | 245.9 ± 82.5 | 225.6 ± 86.5 | 0.016 | 278.7 ± 83.6 | 211.6 ± 73.1 | < 0.001 | 239.3 ± 84.3 |
| Optic disc | | | | | | | |
| Peripapillary atrophy (n) | | | | | | | |
| • None | 21 (6.8%) | 7 (4.7%) | 0.012 | 21 (11.2%) | 7 (2.6%) | < 0.001 | 28 (6.1%) |
| • Mild | 176 (57.1%) | 74 (50.0%) | | 117 (62.2%) | 133 (49.6%) | | 250 (54.8%) |
| • Moderate | 110 (35.7%) | 61 (41.2%) | | 50 (26.6%) | 121 (45.1%) | | 171 (37.5%) |
| • Severe | 1 (0.3%) | 6 (4.1%) | | 0 | 7 (2.6%) | | 7 (1.5%) |
| Disc tilt (n) | | | | | | | |
| • None | 35 (11.4%) | 11 (7.4%) | 0.419 | 34 (18.1%) | 12 (4.5%) | < 0.001 | 46 (10.1%) |
| • Mild | 237 (76.9%) | 117 (79.1%) | | 142 (75.5%) | 212 (79.1%) | | 354 (77.6%) |
| • Moderate | 34 (11.0%) | 20 (13.5%) | | 12 (6.4%) | 42 (15.7%) | | 54 (11.8%) |
| • Severe | 2 (0.6%) | 0 | | 0 | 2 (0.7%) | | 2 (0.4%) |
| Macula | | | | | | | |
| Myopic macular degeneration (n) | | | | | | | |
| • None | 73 (23.7%) | 23 (15.5%) | 0.049 | 68 (36.2%) | 28 (10.4%) | < 0.001 | 96 (21.1%) |
| • Tessellated Fundus | 218 (70.8%) | 111 (75.0%) | | 118 (62.8%) | 211 (78.7%) | | 329 (72.1%) |
| • Diffuse peripapillary/ chorioretinal atrophy | 17 (5.5%) | 13 (8.8%) | | 2 (1.1%) | 28 (10.4%) | | 30 (6.6%) |
| • Patchy chorioretinal atrophy | 0 | 1 (0.7%) | | 0 | 1 (0.4%) | | 1 (0.2%) |
| • Macular atrophy | 0 | 0 | | 0 | 0 | | 0 |
| Plus lesions (n) | 0 | 1 (0.7%) | 0.325 | 0 | 1 (0.4%) | 1.000 | 1 (0.2%) |
| Macular hole (n) | 0 | 1 (0.7%) | 0.325 | 0 | 1 (0.4%) | 1.000 | 1 (0.2%) |
| Myopic tractional maculopathy (n) | 0 | 0 | - | 0 | 0 | - | 0 |
| Retina | | | | | | | |
| Peripheral retina degeneration (n) | | | | | | | |
| • None | 285 (92.5%) | 148 (100.0%) | 0.002 | 180 (95.7%) | 253 (94.4%) | 0.427 | 433 (95.0%) |
| • White without pressure | 12 (3.9%) | 0 | | 3 (1.6%) | 9 (3.4%) | | 12 (2.6%) |
| • Lattice degeneration | 10 (3.2%) | 0 | | 4 (2.1%) | 6 (2.2%) | | 10 (2.2%) |
| • Retinal holes and tears | 1 (0.3%) | 0 | | 1 (0.5%) | 0 | | 1 (0.2%) |
| • Retinal detachment | 0 | 0 | | 0 | 0 | | 0 |
| Retinoschisis (n) | 0 | 3 (2.0%) | 0.034 | 0 | 3 (1.1%) | 0.271 | 3 (0.7%) |
| Posterior staphyloma (n) | 4 (1.3%) | 8 (5.4%) | 0.023 | 0 | 12 (4.5%) | 0.002 | 12 (2.6%) |
| Epiretinal membrane (n) | 2 (0.6%) | 6 (4.1%) | 0.016 | 2 (1.1%) | 6 (2.2%) | 0.480 | 8 (1.8%) |
| Dome shaped macula (n) | 0 | 7 (4.7%) | < 0.001 | 0 | 7 (2.6%) | 0.045 | 7 (1.5%) |
| Intrachoroidal cavitation (n) | 0 | 3 (2.0%) | 0.034 | 2 (1.1%) | 1 (0.4%) | 0.572 | 3 (0.7%) |

Data presented as mean ± standard deviation or number (percentage), where appropriate

N = number of subjects; n = number of eyes

P values in bold indicate statistical significance

[†] P value was estimated based on Chi-squared, Fisher's exact, or independent t-test, where appropriate

Table 2 Agreement and correlation between automated and manual segmented choroidal thickness

| Subjects | n | LOA | | Proportion of outliers (n [%]) | Fixed bias | | P value | Proportional bias (β) | P value | ICC ^a | 95% CI | P value | r | P value |
|------------------------|-----|---------------------------------|---------------------------|--------------------------------|------------|--------------------|--------------|-----------------------|--------------|------------------|----------------|---------|-------|---------|
| | | Lower bound LOA (95% CI) | Upper bound LOA (95% CI) | | 95% CI | 95% CI | | | | | | | | |
| PLEX Elite 9000 | | | | | | | | | | | | | | |
| All subjects | 456 | -47.787 (-52.134 to -43.440) | 60.475 (56.128 to 64.822) | 20 (4.4) | 6.344 | 3.802 to 8.886 | <0.001 | 0.120 | <0.001 | 0.937 | 0.922 to 0.949 | <0.001 | 0.946 | <0.001 |
| AL < 26 mm | 188 | -47.171 (-54.530 to -39.813) | 69.932 (62.574 to 77.291) | 9 (4.8) | 11.380 | 7.083 to 15.679 | <0.001 | 0.098 | <0.001 | 0.921 | 0.878 to 0.947 | <0.001 | 0.934 | <0.001 |
| AL ≥ 26 mm | 268 | -46.943 (-52.168 to -41.719) | 52.565 (47.341 to 57.789) | 8 (3.0) | 2.811 | -0.242 to 5.864 | 0.071 | 0.134 | <0.001 | 0.931 | 0.913 to 0.946 | <0.001 | 0.940 | <0.001 |
| ChT < 300 μm | 371 | -46.524 (-50.955 to -42.940) | 52.923 (48.493 to 57.353) | 13 (3.5) | 3.199 | 0.610 to 5.789 | 0.016 | 0.158 | <0.001 | 0.890 | 0.866 to 0.909 | <0.001 | 0.901 | <0.001 |
| ChT ≥ 300 μm | 85 | -43.815 (-55.877 to -31.753) | 83.952 (71.890 to 96.014) | 6 (7.1) | 20.068 | 13.038 to 27.099 | <0.001 | -0.011 | 0.881 | 0.749 | 0.492 to 0.864 | <0.001 | 0.803 | <0.001 |
| Triton DRI-OCT | | | | | | | | | | | | | | |
| All subjects | 456 | -90.556 (-95.683 to -85.429) | 37.127 (32.000 to 42.254) | 30 (6.6) | -26.714 | -29.711 to -23.716 | <0.001 | -0.090 | <0.001 | 0.887 | 0.608 to 0.950 | <0.001 | 0.933 | <0.001 |
| AL < 26 mm | 188 | -105.076 (-114.522 to -95.629) | 45.258 (35.811 to 54.704) | 11 (5.9) | -29.908 | -35.426 to -24.391 | <0.001 | -0.108 | 0.001 | 0.852 | 0.555 to 0.931 | <0.001 | 0.907 | <0.001 |
| AL ≥ 26 mm | 268 | -78.709 (-84.403 to -73.014) | 29.762 (24.067 to 35.456) | 14 (5.2) | -24.473 | -27.801 to -21.145 | <0.001 | -0.077 | <0.001 | 0.884 | 0.545 to 0.952 | <0.001 | 0.934 | <0.001 |
| ChT < 300 μm | 375 | -77.249 (-82.020 to -72.479) | 30.419 (25.648 to 35.189) | 17 (4.5) | -23.415 | -26.204 to -20.626 | <0.001 | -0.011 | 0.666 | 0.830 | 0.453 to 0.924 | <0.001 | 0.894 | <0.001 |
| ChT ≥ 300 μm | 81 | -134.339 (-152.218 to -116.461) | 50.362 (32.484 to 68.241) | 6 (7.4) | -41.987 | -52.406 to -31.569 | <0.001 | -0.328 | <0.001 | 0.561 | 0.090 to 0.778 | <0.001 | 0.723 | <0.001 |

P values in bold indicate statistical significance

n = number of eyes; LOA = limits of agreement; β = unstandardized coefficient; r = Pearson correlation coefficient; ICC = intraclass correlation coefficient; AL = axial length; ChT = choroidal thickness
^a ICC was calculated based on two-way mixed effects absolute agreement model

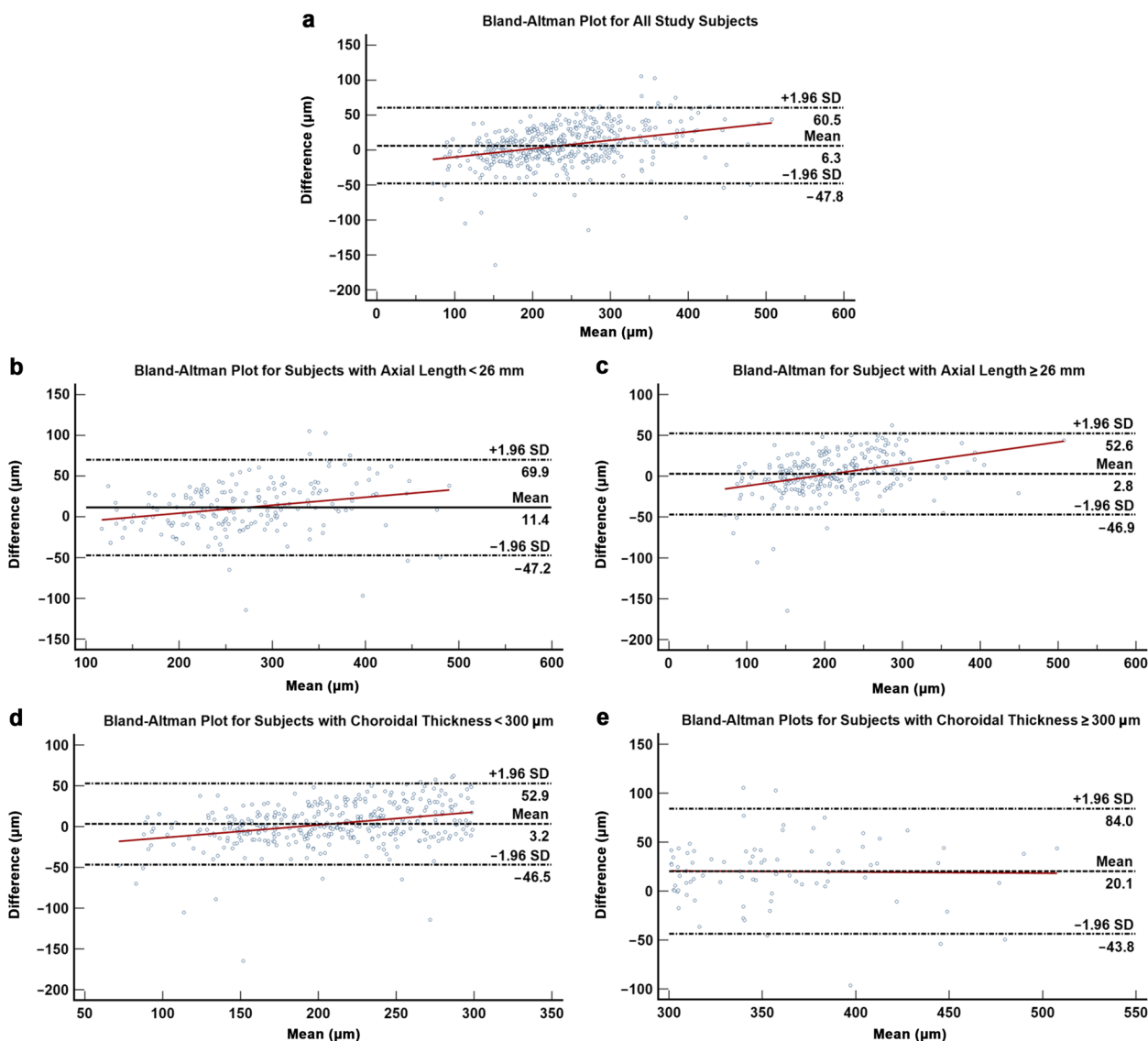


Fig. 2 Bland–Altman plot demonstrating the agreement between automated and manual segmented choroidal thickness measurements for PLEX Elite 9000. **a** All subjects; **b, c** Subjects with axial length less than and more than 26 mm, respectively; **d, e** Subjects with choroidal thickness less than and more than 300 μm, respectively

Table 3 summarizes the indices for agreement and correlation between Triton DRI-OCT and PLEX Elite 9000 for manual-segmented choroidal thickness measurement. ICC (0.930, 95% CI: 0.602 to 0.974, $P < 0.001$) and Pearson correlation coefficient ($r = 0.964$, $P < 0.001$) demonstrated excellent agreement and correlation between both SS-OCT modalities. Triton DRI-OCT choroidal thickness measurements were comparatively thinner than PLEX Elite 9000, with a fixed bias of $-22.363 \mu\text{m}$ (95% CI: -24.435 to -20.291 , $P < 0.001$, 95% LOA: -66.501 to 21.775 ; Fig. 4a). Nevertheless, there was no statistically

significant proportional bias ($P = 0.126$) between the two SS-OCT modalities. Following stratification for axial length (< 26 mm versus ≥ 26 mm), the inter-modality agreement and correlation coefficient remained excellent in both subgroups. Subjects with axial length < 26 mm (fixed bias = -23.457 , 95% CI: -27.439 to -19.476 , $P < 0.001$, 95% LOA: -77.698 to 30.783) showed a larger magnitude of fixed bias as compared to subjects with axial length ≥ 26 mm (fixed bias = -21.595 , 95% CI: -23.768 to -19.422 , $P < 0.001$, 95% LOA: -57.005 to 13.815 ; Fig. 4b and c). No proportional bias was observed

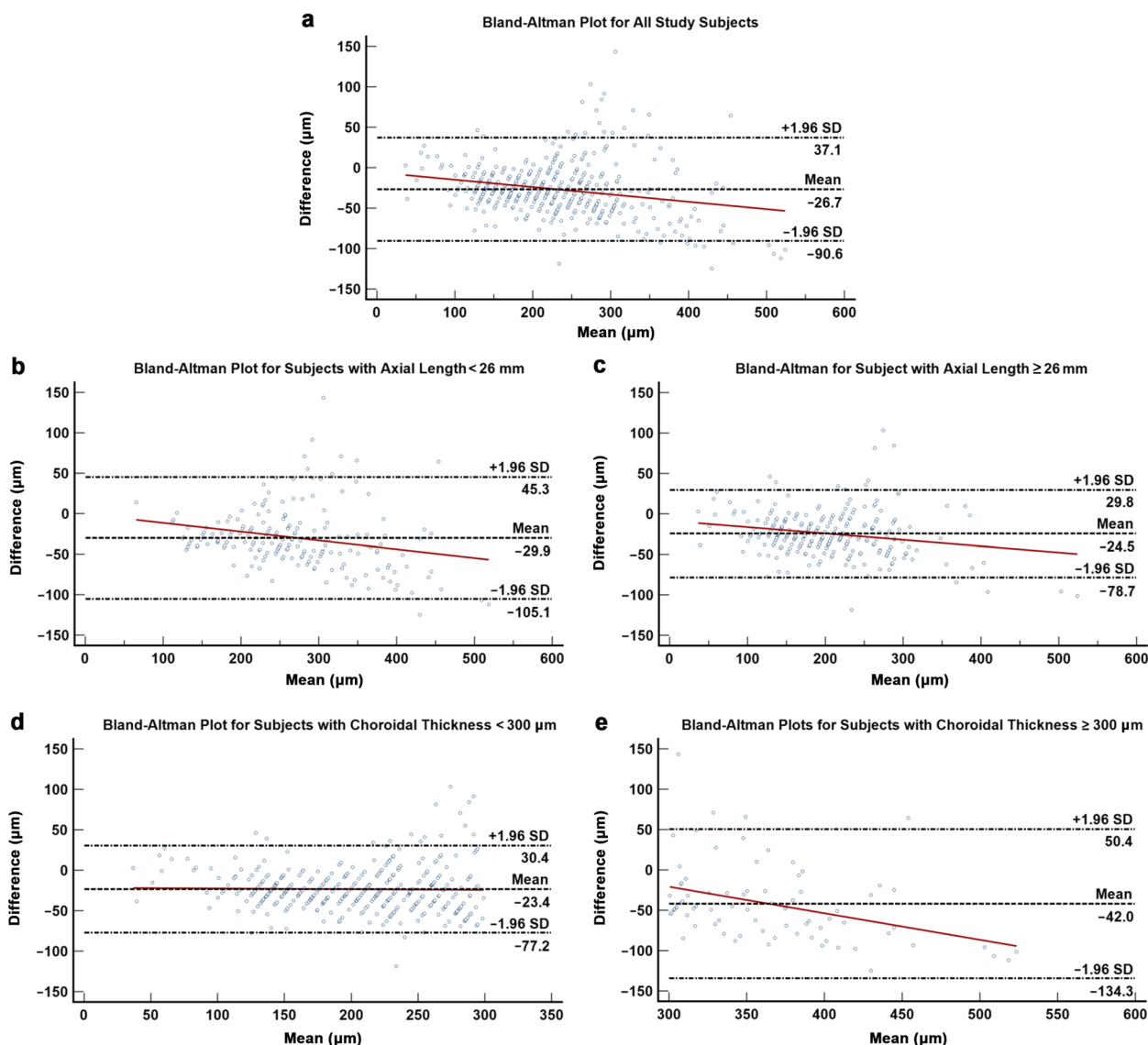


Fig. 3 Bland–Altman plot demonstrating the agreement between automated and manual segmented choroidal thickness measurements for DRI-OCT. **a** All subjects; **b, c** Subjects with axial length less than and more than 26 mm, respectively; **d, e** Subjects with choroidal thickness less than and more than 300 μm, respectively

in either subgroup (all $P \geq 0.273$). On the contrary, when the analysis was stratified for choroidal thickness, subjects with choroidal thickness $\geq 300 \mu\text{m}$ ($\text{ICC} = 0.759$, 95% CI: 0.175 to 0.905, $P < 0.001$; $r = 0.866$, $P < 0.001$) demonstrated weaker correlation and agreement as compared to those with choroidal thickness $< 300 \mu\text{m}$ ($\text{ICC} = 0.874$, 95% CI: 0.423 to 0.951, $P < 0.001$; $r = 0.932$, $P < 0.001$). Notably, the magnitude of fixed bias was larger in subjects with choroidal thickness $\geq 300 \mu\text{m}$ (fixed bias = -26.512 , 95% CI: -32.241 to -20.783 , $P < 0.001$, 95% LOA: -77.295 to 24.270 versus fixed bias = -21.467 , 95% CI: -23.665 to -19.268 , $P < 0.001$,

95% LOA: -63.906 to 20.972 ; Fig. 4d and e). Proportional bias was statistically insignificant in both subgroups (all $P \geq 0.421$).

Discussion

In our study of myopic adults, we observed a mean choroidal thickness of $216.9 \mu\text{m}$ and $239.3 \mu\text{m}$ measured by the Triton DRI-OCT and PLEX Elite 9000, respectively. Both modalities exhibited excellent agreement between automated (SA-Net) and manual segmented choroidal thickness measurements in myopic adults with a range of different axial lengths. Notably, the magnitude

Table 3 Agreement and correlation between triton DRI-OCT and PLEX Elite 9000 for manual-segmented choroidal thickness measurement

| Subjects | n | LOA | | Proportion of outliers (n [%]) | Fixed bias | 95% CI | P value | Proportional bias (β) | P value | ICC ^a | 95% CI | r | P value |
|--------------|-----|------------------------------|---------------------------|--------------------------------|------------|--------------------|---------|-----------------------|---------|------------------|----------------|-------|---------|
| | | Lower bound LOA (95% CI) | Upper bound LOA (95% CI) | | | | | | | | | | |
| All subjects | 456 | -66.501 (-70.045 to -62.957) | 21.775 (18.231 to 25.320) | 23 (5.0) | -22.363 | -24.435 to -20.291 | <0.001 | -0.020 | 0.126 | 0.930 | 0.602 to 0.974 | 0.964 | <0.001 |
| AL < 26 mm | 188 | -77.698 (-84.515 to -70.882) | 30.783 (23.967 to 37.600) | 7 (3.7) | -23.457 | -27.439 to -19.476 | <0.001 | -0.019 | 0.442 | 0.908 | 0.639 to 0.961 | 0.944 | <0.001 |
| AL ≥ 26 mm | 268 | -57.005 (-60.723 to -53.287) | 13.815 (10.097 to 17.533) | 18 (6.7) | -21.595 | -23.768 to -19.422 | <0.001 | -0.017 | 0.273 | 0.928 | 0.416 to 0.976 | 0.969 | <0.001 |
| ChT < 300 μm | 375 | -63.906 (-67.666 to -60.145) | 20.972 (17.211 to 24.733) | 14 (3.7) | -21.467 | -23.665 to -19.268 | <0.001 | 0.001 | 0.946 | 0.874 | 0.423 to 0.951 | 0.932 | <0.001 |
| ChT ≥ 300 μm | 81 | -77.295 (-87.126 to -67.464) | 24.270 (14.439 to 34.102) | 4 (4.9) | -26.512 | -32.241 to -20.783 | <0.001 | -0.049 | 0.421 | 0.759 | 0.175 to 0.905 | 0.866 | <0.001 |

P values in bold indicate statistical significance

n = number of eyes; LOA = limits of agreement; β = unstandardized coefficient; r = Pearson correlation coefficient; ICC = intraclass correlation coefficient; AL = axial length; ChT = choroidal thickness

^a ICC was calculated based on two-way mixed effects, absolute agreement model

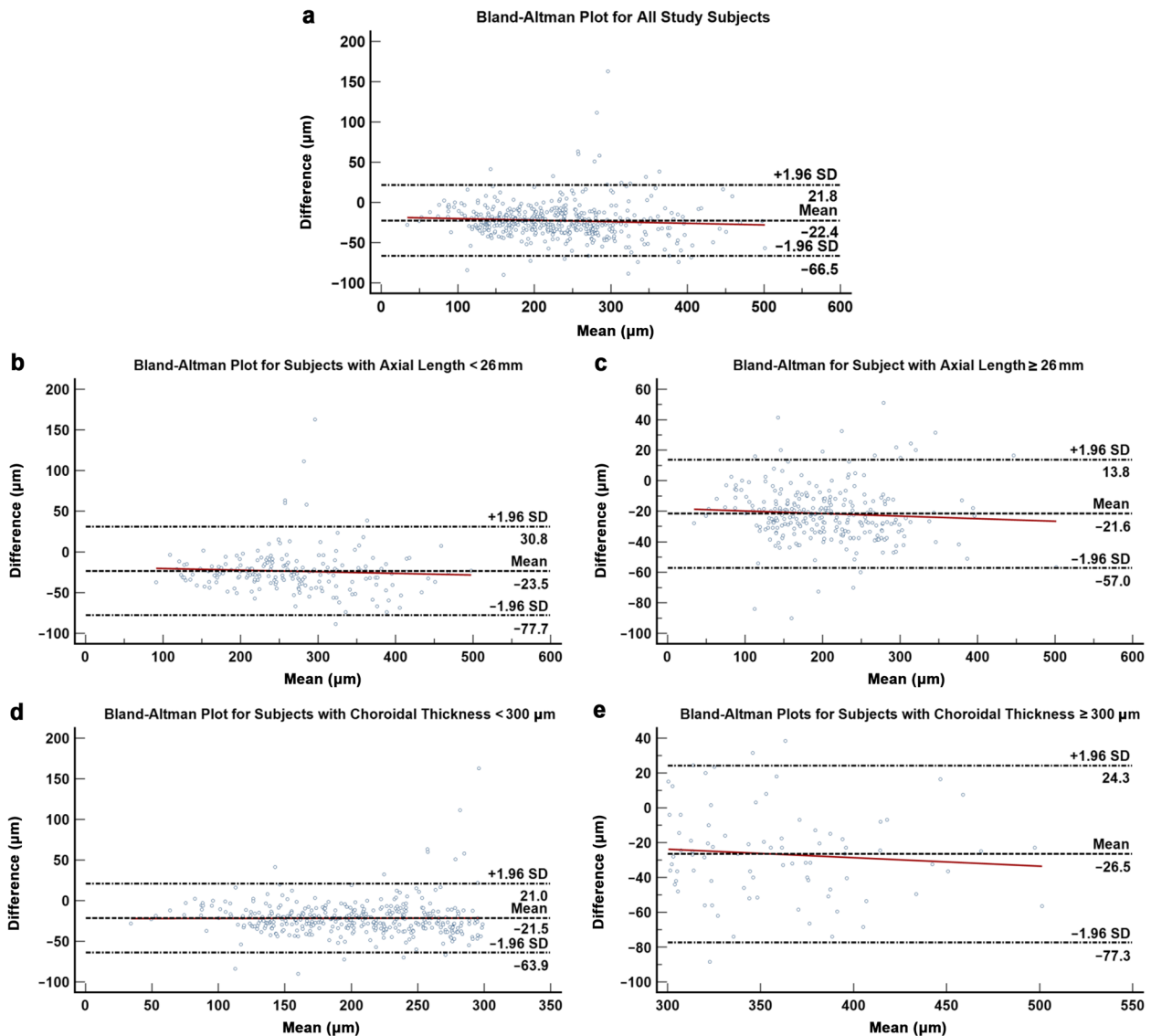


Fig. 4 Bland–Altman plot demonstrating the agreement between Triton DRI-OCT and PLEX Elite 9000 for choroidal thickness measurements. **a** all subjects; **b, c** Subjects with axial length less than and more than 26 mm, respectively; **d, e** Subjects with choroidal thickness less than and more than 300 µm, respectively

of agreement was markedly lower in eyes with thicker choroids ($\geq 300 \mu\text{m}$). Choroidal thickness measurements by both SS-OCT modalities were also comparable with excellent agreement indices. To the best of our knowledge, our study is the first to demonstrate the agreement between these measurements. Our findings contribute further insights into the normative choroidal thickness amongst a population of myopes and provide further clarification towards the clinical utility of SA-Net and interchangeability of choroidal thickness measurements across different SS-OCT modalities.

Several studies have described the normative profiles of choroidal thickness in myopic eyes [7, 40–49]. Given the heterogenous subject characteristics and study methodologies (OCT modality and myopia definition), it is challenging to compare our mean choroidal thickness values with other studies. However, we were able to replicate the previously demonstrated relationships between both increased age and axial length with thinner choroidal thickness [7, 40–49]. When we further stratified the analysis based on ETDRS grid areas, we observed that choroidal thickness was thinnest in the nasal macular region

(Supplementary Table 1), consistent with several other studies [47–54]. This may be explained by the choroid's watershed zone, which is located between the optic disc and the fovea [55, 56]. Interestingly, following adjustment for age and gender, we also observed that the change in choroidal thickness per unit change in axial length was the greatest in the inferior macular regions (Supplementary Table 2; $\beta = -29.188$ and $\beta = -28.256$ in the inner and outer macular areas, respectively), suggesting that these areas could be more susceptible to stretching and subsequent thinning with axial length elongation. However, due to the cross-sectional nature of our study, further longitudinal studies are necessary to validate these hypotheses.

AI has recently garnered significant interest in ophthalmology, driving the automation of several clinical processes [57–65]. In this regard, several deep-learning based approaches have been proposed for the segmentation of 3D volumetric data such as OCT images [28–31]. Nonetheless, the majority of these methods require extensive computational memory and long processing time, making them less feasible to adopt in the clinical setting. Cahyo et al. have introduced a novel multi-task learning approach – SA-Net, targeted towards addressing these limitations [28]. We compared our manual segmented choroidal thickness measurements to those segmented by SA-Net [28] and observed an excellent agreement, albeit with an exception in subjects with choroidal thickness ≥ 300 μm . Importantly, patients with thinner choroids are more at risk of pathology, and thus our results hold well for the targeted patient population, which would be followed more closely in a clinical setting.

As proposed by Tan et al., a thicker choroid may result in higher signal loss and more artefacts owing to a larger amount of interstitial connective tissue [20]. In this regard, visualization of the choroidal–scleral interface may be impacted, thereby leading to greater variability during manual segmentation [24]. On the contrary, Cahyo et al. evaluated the accuracy of segmentation volume and resemblance of thickness map with respect to ground truth segmentation and observed better segmentation performance in thicker choroids (≥ 300 μm) across all AI-driven architectures [28]. Collectively, this may suggest that the visibility of Bruch's membrane and choroidal–scleral interface perceived by the human eye and AI may depend on different factors and choroidal thickness measurements in subjects with thicker choroid may be more accurate with SA-Net.

Apart from being able to perform automated choroidal segmentation with comparable accuracy to manual

segmentation, Cahyo et al.'s novel algorithm also possesses the intrinsic advantage accompanied with AI – superior repeatability, reduced grader variability, and less labour intensiveness. Considering its strengths, automated segmentation may become the mainstay method for determining choroidal thickness clinically. Nonetheless, future studies are necessary to further evaluate this aspect.

Our secondary aim was to evaluate the correlation and agreement between two well-established SS-OCT modalities – Triton DRI-OCT and PLEX Elite 9000. In terms of correlation, our findings ($r = 0.964$, $P < 0.001$) were consistent with Marengo et al.'s study, which also found an excellent correlation between choroidal thickness measurements from both modalities ($r = 0.944$, $P < 0.001$), albeit in a study population of subjects with primary open-angle glaucoma [66]. Although the agreement between both modalities was determined to be excellent in our study, clinicians should be cognizant of the inter-modality fixed bias (-22.363 μm), particularly in selected clinical context. For instance, in OCT-based staging of MMD, choroidal thickness for peripapillary and macular diffuse choroidal atrophy was 84.6 μm and 50.2 μm , respectively, and thus a magnitude of -22.363 μm may well be significant in evaluating pathologic myopes [15].

We postulate that this fixed bias may be attributed to the differences in the axial resolution of these modalities – 8 μm in Triton DRI-OCT versus 6.3 μm in PLEX Elite 9000 [35, 36]. The axial resolution, as defined by the ability to distinguish between two distinct objects which are positioned adjacent to each other in the longitudinal plane, may influence the visualization of the true choroidal–scleral interface. In this regard, measurements derived from the PLEX Elite 9000 may potentially be a closer representation of the true choroidal thickness. Nevertheless, further studies are warranted to ascertain this finding.

Based on previous OCT studies, axial length was found to have an impact on the optical magnification and accuracy of OCT-derived ocular parameters, namely due to transverse magnification from axial length [67, 68]. Hence, we stratified our analysis to elucidate the effect of axial length on the agreement between two modalities. We found minimal differences in Pearson correlation coefficient and ICC, suggesting that both modalities may be equally affected in this aspect. We also stratified our analysis for choroidal thickness and observed weaker correlation and agreement indices in subjects with thicker choroids (≥ 300 μm), albeit still high with a coefficient of 0.866 and 0.759 , respectively. Furthermore, subjects with thicker choroids also showed a larger magnitude of fixed

bias, suggesting more variability within measurements. As discussed earlier in this section, this may be due to the higher signal loss and increased artefacts associated with thicker choroids [20, 24]. Taken together, inter-modality choroidal thickness measurements must be interpreted with care in subjects with thicker choroids.

The strengths of our study include its large sample size of myopic subjects with a broad range of axial length and spherical equivalent. Furthermore, a robust study design with standardized methodology was adopted, with conscious efforts to reduce intra- and inter-grader variability. To our knowledge, this is the first study comparing choroidal thickness measurements in these two commonly used imaging modalities. Nevertheless, our study has its limitations. Our study lacks representation from older subjects, who might be the more important target population given their higher risk of thin choroid and pathologic myopia. Moreover, our study population is generally healthy with an average visual acuity of 0.02 LogMAR, so these results may not be generalizable to those with ocular disease such as pathologic myopia. The exclusion of images of poor quality from our study might also limit the generalizability of our findings to real-world clinical scenarios, where encountering poor-quality images is inevitable, particularly in high myopes with anatomical variances such as staphyloma, DSM, and severe choroidal thinning. Notably, both SS-OCT modalities adopted significantly different imaging protocol. Given that the imaging protocols are proprietary to respective manufacturers, this is an inherent limitation within our study. Nonetheless, this mirrors a real-world scenario encountered in the clinical settings, where different modalities often employ distinct imaging protocols. In this regard, SA-Net only analyses the foveal and macular area (Fig. 1), meaning the difference in scan dimensions between Triton DRI-OCT and PLEX Elite 9000 (3.0×3.0 mm versus 7.0×7.0 mm) is unlikely to impact the comparison between modalities. We also did not directly correct for transverse magnification due to axial length, although both modalities would be affected by this bias. Furthermore, due to the lack of topographical choroidal thickness data from the PLEX Elite 9000, we were only able to ascertain the agreement and correlation between Triton DRI-OCT and PLEX Elite 9000 for subfoveal choroidal thickness. Further studies examining choroidal thickness data across the macular region are warranted to validate this aspect. It is essential to acknowledge that SA-Net assumed the foveal location to be precisely at the center of the images. Although most images were generally well-centered in our study, this could potentially introduce minor offsets, which could have affected the accuracy of SFCT measurements. Future studies may utilise adjunctive registration software to improve fovea detection and

accuracy of SFCT measurements. Our study would have also provided more insight by including time as an objective measure, allowing for an evaluation of the differences in duration required for manual versus automated segmentation. Lastly, as manual segmented choroidal thickness measurements were performed with callipers, issues with repeatability cannot be excluded.

Conclusion

Choroidal thickness measurements using manual and automated (SA-Net) segmentation are comparable among adults with myopia. Given its edge over manual segmentation, automated segmentation may further enhance the clinical utility of choroidal thickness in myopia management and emerge as the primary method of measurement in the future.

Supplementary Information

The online version contains supplementary material available at <https://doi.org/10.1186/s40662-024-00385-2>.

Additional file 1: Supplementary Figure 1. Protocol for the manual measurement of choroidal thickness with Triton DRI-OCT and PLEX Elite 9000.

Additional file 2: Supplementary Table 1. Choroidal thickness measured with Triton DRI-OCT, across Early Treatment Diabetic Retinopathy Study (ETDRS) grid areas.

Additional file 3: Supplementary Table 2. Multivariable linear regression with linear mixed model analysis on the associations between age, gender, and axial length with choroidal thickness across the ETDRS grid areas.

Acknowledgements

Not applicable.

Authors' contributions

ZWL, JL, MA contributed to conception of the study and study design. ZWL, DW, JC, AT contributed to acquisition of the data. ZWL, JL, MA contributed to statistical analysis and interpretation of the data. ZWL, MA contributed to visualisation which includes figures and tables of the data. ZWL, JL, MA drafted the manuscript. All authors read and approved the final version of the manuscript.

Funding

Singapore Eye Research Institute - Johnson & Johnson Vision Care Joint Research Programme for Myopia, Industry Alignment Fund – Industry Collaboration Project (ICP-1700052).

Availability of data and materials

The datasets used and/or analysed in this current study are available from the corresponding author on reasonable request.

Declarations

Ethics approval and consent to participate

Ethics approval was obtained from the Centralized Institutional Review Board of Singapore Health Services (CIRB Reference Number: 2019/2069). Written informed consent was obtained from all subjects.

Consent for publication

Not applicable.

Competing interests

The authors declare that they have no competing interests.

Author details

¹Yong Loo Lin School of Medicine, National University of Singapore, Singapore, Singapore. ²Department of Ophthalmology, University of California, San Francisco, CA, USA. ³Singapore Eye Research Institute, Singapore National Eye Centre, Singapore, Singapore. ⁴Ophthalmology and Visual Sciences Department, Duke-NUS Medical School, Singapore, Singapore. ⁵SERI-NTU Advanced Ocular Engineering (STANCE), Singapore Eye Research Institute and Nanyang Technological University, Singapore, Singapore. ⁶Center for Medical Physics and Biomedical Engineering, Medical University Vienna, Vienna, Austria. ⁷Duke-NUS Medical School, National University of Singapore, Singapore, Singapore. ⁸Institute of Molecular and Clinical Ophthalmology, Basel, Switzerland. ⁹Department of Ophthalmology, Yong Loo Lin School of Medicine, National University of Singapore, Singapore, Singapore. ¹⁰Department of Ophthalmology, Edward S. Harkness Eye Institute, Columbia University Vagelos College of Physicians and Surgeons, New York, NY, USA. ¹¹Saw Swee Hock School of Public Health, National University of Singapore, Singapore, Singapore. ¹²School of Chemistry, Chemical Engineering and Biotechnology, Nanyang Technological University, Singapore, Singapore. ¹³Department of Clinical Pharmacology, Medical University Vienna, Vienna, Austria. ¹⁴Johnson & Johnson Vision, Jacksonville, FL, USA.

Received: 18 October 2023 Accepted: 17 April 2024

Published online: 03 June 2024

References

- Holden BA, Fricke TR, Wilson DA, Jong M, Naidoo KS, Sankaridurg P, et al. Global prevalence of myopia and high myopia and temporal trends from 2000 through 2050. *Ophthalmology*. 2016;123(5):1036–42.
- Wong TY, Ferreira A, Hughes R, Carter G, Mitchell P. Epidemiology and disease burden of pathologic myopia and myopic choroidal neovascularization: an evidence-based systematic review. *Am J Ophthalmol*. 2014;157(1):9–25.e12.
- Saw SM, Gazzard G, Shih-Yen EC, Chua WH. Myopia and associated pathological complications. *Ophthalmic Physiol Opt*. 2005;25(5):381–91.
- Sanchez-Cano A, Orduña E, Segura F, Lopez C, Cuenca N, Abecia E, et al. Choroidal thickness and volume in healthy young white adults and the relationships between them and axial length, ametropia and sex. *Am J Ophthalmol*. 2014;158(3):574–83.e1.
- Jin P, Zou H, Xu X, Chang TC, Zhu J, Deng J, et al. Longitudinal changes in choroidal and retinal thicknesses in children with myopic shift. *Retina*. 2019;39(6):1091–9.
- Read SA, Alonso-Caneiro D, Vincent SJ, Collins MJ. Longitudinal changes in choroidal thickness and eye growth in childhood. *Invest Ophthalmol Vis Sci*. 2015;56(5):3103–12.
- Ho M, Liu DT, Chan VC, Lam DS. Choroidal thickness measurement in myopic eyes by enhanced depth optical coherence tomography. *Ophthalmology*. 2013;120(9):1909–14.
- Nishida Y, Fujiwara T, Imamura Y, Lima LH, Kurosaka D, Spaide RF. Choroidal thickness and visual acuity in highly myopic eyes. *Retina*. 2012;32(7):1229–36.
- Wong CW, Phua V, Lee SY, Wong TY, Cheung CM. Is choroidal or scleral thickness related to myopic macular degeneration? *Invest Ophthalmol Vis Sci*. 2017;58(2):907–13.
- Wei WB, Xu L, Jonas JB, Shao L, Du KF, Wang S, et al. Subfoveal choroidal thickness: the Beijing Eye Study. *Ophthalmology*. 2013;120(1):175–80.
- Esmaelpour M, Povazay B, Hermann B, Hofer B, Kujic V, Kapoor K, et al. Three-dimensional 1060-nm OCT: choroidal thickness maps in normal subjects and improved posterior segment visualization in cataract patients. *Invest Ophthalmol Vis Sci*. 2010;51(10):5260–6.
- Ouyang Y, Heussen FM, Mokwa N, Walsh AC, Durbin MK, Keane PA, et al. Spatial distribution of posterior pole choroidal thickness by spectral domain optical coherence tomography. *Invest Ophthalmol Vis Sci*. 2011;52(9):7019–26.
- Tan CS, Cheong KX. Macular choroidal thicknesses in healthy adults—relationship with ocular and demographic factors. *Invest Ophthalmol Vis Sci*. 2014;55(10):6452–8.
- Read SA, Fuss JA, Vincent SJ, Collins MJ, Alonso-Caneiro D. Choroidal changes in human myopia: insights from optical coherence tomography imaging. *Clin Exp Optom*. 2019;102(3):270–85.
- Fang Y, Du R, Nagaoka N, Yokoi T, Shinohara K, Xu X, et al. OCT-based diagnostic criteria for different stages of myopic maculopathy. *Ophthalmology*. 2019;126(7):1018–32.
- Xie R, Qiu B, Chhablani J, Zhang X. Evaluation of choroidal thickness using optical coherent tomography: a review. *Front Med (Lausanne)*. 2021;8:783519.
- Spaide RF, Koizumi H, Pozzoni MC. Enhanced depth imaging spectral-domain optical coherence tomography. *Am J Ophthalmol*. 2008;146(4):496–500.
- Philip AM, Gerendas BS, Zhang L, Faatz H, Podkowinski D, Bogunovic H, et al. Choroidal thickness maps from spectral domain and swept source optical coherence tomography: algorithmic versus ground truth annotation. *Br J Ophthalmol*. 2016;100(10):1372–6.
- Adhi M, Liu JJ, Qavi AH, Grulkowski I, Lu CD, Mohler KJ, et al. Choroidal analysis in healthy eyes using swept-source optical coherence tomography compared to spectral domain optical coherence tomography. *Am J Ophthalmol*. 2014;157(6):1272–81.e1.
- Tan CS, Ngo WK, Cheong KX. Comparison of choroidal thicknesses using swept source and spectral domain optical coherence tomography in diseased and normal eyes. *Br J Ophthalmol*. 2015;99(3):354–8.
- Zafar S, Siddiqui MR, Shahzad R. Comparison of choroidal thickness measurements between spectral-domain OCT and swept-source OCT in normal and diseased eyes. *Clin Ophthalmol*. 2016;10:2271–6.
- Matsuo Y, Sakamoto T, Yamashita T, Tomita M, Shirasawa M, Terasaki H. Comparisons of choroidal thickness of normal eyes obtained by two different spectral-domain OCT instruments and one swept-source OCT instrument. *Invest Ophthalmol Vis Sci*. 2013;54(12):7630–6.
- Narendran S, Manayath G, Venkatapathy N. Comparison of choroidal thickness using swept-source and spectral-domain optical coherence tomography in normal Indian eyes. *Oman J Ophthalmol*. 2018;11(1):38–41.
- Lee MW, Park HJ, Shin YI, Lee WH, Lim HB, Kim JY. Comparison of choroidal thickness measurements using swept source and spectral domain optical coherence tomography in pachychoroid diseases. *PLoS One*. 2020;15(2):e0229134.
- Lee CO, Zhang X, Yuan N, Tang S, Chen LJ, Cheung CY, et al. Comparison of choroidal thickness measurements between spectral domain optical coherence tomography and swept source optical coherence tomography in children. *Sci Rep*. 2021;11(1):13749.
- Yamashita T, Yamashita T, Shirasawa M, Arimura N, Terasaki H, Sakamoto T. Repeatability and reproducibility of subfoveal choroidal thickness in normal eyes of Japanese using different SD-OCT devices. *Invest Ophthalmol Vis Sci*. 2012;53(3):1102–7.
- Branchini L, Regatieri CV, Flores-Moreno I, Baumann B, Fujimoto JG, Duker JS. Reproducibility of choroidal thickness measurements across three spectral domain optical coherence tomography systems. *Ophthalmology*. 2012;119(1):119–23.
- Cahyo DAY, Yow AP, Saw SM, Ang M, Girard M, Schmetterer R, et al. Multi-task learning approach for volumetric segmentation and reconstruction in 3D OCT images. *Biomed Opt Express*. 2021;12(12):7348–60.
- Dou Q, Yu L, Chen H, Jin Y, Yang X, Qin J, et al. 3D deeply supervised network for automated segmentation of volumetric medical images. *Med Image Anal*. 2017;41:40–54.
- Milletari F, Navab N, Ahmadi SA. V-Net: fully convolutional neural networks for volumetric medical image segmentation. Fourth International Conference on 3D Vision (3DV). 2016. p. 565–71. <https://doi.org/10.48550/arXiv.1606.04797>.
- Çiçek Ö, Abdulkadir A, Lienkamp SS, Brox T, Ronneberger O. 3D U-Net: learning dense volumetric segmentation from sparse annotation. International Conference on Medical Image Computing and Computer-Assisted Intervention. 2016. p. 424–32. <https://doi.org/10.48550/arXiv.1606.06650>.
- Flitcroft DI, He M, Jonas JB, Jong M, Naidoo K, Ohno-Matsui K, et al. IMI - Defining and classifying myopia: a proposed set of standards for clinical and epidemiologic studies. *Invest Ophthalmol Vis Sci*. 2019;60(3):M20–30.
- Ohno-Matsui K, Kawasaki R, Jonas JB, Cheung CM, Saw SM, Verhoeven VJ, et al. International photographic classification and grading system for myopic maculopathy. *Am J Ophthalmol*. 2015;159(5):877–83.e7.
- Tan CS, Ouyang Y, Ruiz H, Sadda SR. Diurnal variation of choroidal thickness in normal, healthy subjects measured by spectral domain optical coherence tomography. *Invest Ophthalmol Vis Sci*. 2012;53(1):261–6.

35. Topcon. DRI OCT-1 (Model Triton) - User Manual. 2015. https://www.topcon.ca/wp-content/uploads/2016/12/DRI-OCT-1-Model-Triton_Triton-plus-Instrument-Manual.pdf. Accessed 10 Jan 2024.
36. Carl Zeiss Meditec. PLEX Elite 9000 - Instructions for Use. 2018. <https://www.zeiss.com/meditec/en/products/optical-coherence-tomography-devices/plex-elite-9000-swept-source-oct.html>. Accessed 10 Jan 2024.
37. Early Treatment Diabetic Retinopathy Study Research Group. Grading diabetic retinopathy from stereoscopic color fundus photographs—an extension of the modified Airline House classification. ETDRS report number 10. *Ophthalmology*. 1991;98(5 Suppl):786–806.
38. Bland JM, Altman DG. Statistical methods for assessing agreement between two methods of clinical measurement. *Lancet*. 1986;1(8476):307–10.
39. Koo TK, Li MY. A guideline of selecting and reporting intraclass correlation coefficients for reliability research. *J Chiropr Med*. 2016;15(2):155–63.
40. Fujiwara T, Imamura Y, Margolis R, Slakter JS, Spaide RF. Enhanced depth imaging optical coherence tomography of the choroid in highly myopic eyes. *Am J Ophthalmol*. 2009;148(3):445–50.
41. Coscas G, Zhou Q, Coscas F, Zucchiatti I, Rispoli M, Uzzan J, et al. Choroid thickness measurement with RTVue optical coherence tomography in emmetropic eyes, mildly myopic eyes, and highly myopic eyes. *Eur J Ophthalmol*. 2012;22(6):992–1000.
42. Hoseini-Yazdi H, Vincent SJ, Collins MJ, Read SA, Alonso-Caneiro D. Wide-field choroidal thickness in myopes and emmetropes. *Sci Rep*. 2019;9(1):3474.
43. Wang S, Wang Y, Gao X, Qian N, Zhuo Y. Choroidal thickness and high myopia: a cross-sectional study and meta-analysis. *BMC Ophthalmol*. 2015;15:70.
44. Teberik K, Kaya M. Retinal and choroidal thickness in patients with high myopia without maculopathy. *Pak J Med Sci*. 2017;33(6):1438–43.
45. El-Shazly AA, Farweez YA, ElSebaay ME, El-Zawahry WMA. Correlation between choroidal thickness and degree of myopia assessed with enhanced depth imaging optical coherence tomography. *Eur J Ophthalmol*. 2017;27(5):577–84.
46. Flores-Moreno I, Lugo F, Duker JS, Ruiz-Moreno JM. The relationship between axial length and choroidal thickness in eyes with high myopia. *Am J Ophthalmol*. 2013;155(2):314–9.e1.
47. Duan F, Yuan Z, Deng J, Wong YL, Yeo AC, Chen X. Choroidal thickness and associated factors among adult myopia: a baseline report from a medical university student cohort. *Ophthalmic Epidemiol*. 2019;26(4):244–50.
48. Gupta P, Saw SM, Cheung CY, Girard MJ, Mari JM, Bhargava M, et al. Choroidal thickness and high myopia: a case-control study of young Chinese men in Singapore. *Acta ophthalmol*. 2015;93(7):e585–92.
49. Zhang Q, Neitz M, Neitz J, Wang RK. Geographic mapping of choroidal thickness in myopic eyes using 1050-nm spectral domain optical coherence tomography. *J Innov Opt Health Sci*. 2015;8(4):1550012.
50. Breher K, Ohlendorf A, Wahl S. A metrological approach to the analysis of choroidal thickness by optical coherence tomography 3D scans in myopia research. *Sci Rep*. 2019;9(1):20322.
51. Tan CS, Cheong KX, Lim LW, Li KZ. Topographic variation of choroidal and retinal thicknesses at the macula in healthy adults. *Br J Ophthalmol*. 2014;98(3):339–44.
52. Ikuno Y, Tano Y. Retinal and choroidal biometry in highly myopic eyes with spectral-domain optical coherence tomography. *Invest Ophthalmol Vis Sci*. 2009;50(8):3876–80.
53. Goldenberg D, Moisseiev E, Goldstein M, Loewenstein A, Barak A. Enhanced depth imaging optical coherence tomography: choroidal thickness and correlations with age, refractive error, and axial length. *Ophthalmic Surg Lasers Imaging*. 2012;43(4):296–301.
54. Ding X, Li J, Zeng J, Ma W, Liu R, Li T, et al. Choroidal thickness in healthy Chinese subjects. *Invest Ophthalmol Vis Sci*. 2011;52(13):9555–60.
55. Giuffrè G. Main posterior watershed zone of the choroid. Variations of its position in normal subjects. *Doc Ophthalmol*. 1989;72(2):175–80.
56. Hayreh SS. In vivo choroidal circulation and its watershed zones. *Eye (London)*. 1990;4(Pt 2):273–89.
57. Wu X, Huang Y, Liu Z, Lai W, Long E, Zhang K, et al. Universal artificial intelligence platform for collaborative management of cataracts. *Br J Ophthalmol*. 2019;103(11):1553–60.
58. Ting DSW, Cheung CY, Lim G, Tan GSW, Quang ND, Gan A, et al. Development and validation of a deep learning system for diabetic retinopathy and related eye diseases using retinal images from multiethnic populations with diabetes. *JAMA*. 2017;318(22):2211–23.
59. Gulshan V, Peng L, Coram M, Stumpe MC, Wu D, Narayanaswamy A, et al. Development and validation of a deep learning algorithm for detection of diabetic retinopathy in retinal fundus photographs. *JAMA*. 2016;316(22):2402–10.
60. Gargeya R, Leng T. Automated identification of diabetic retinopathy using deep learning. *Ophthalmology*. 2017;124(7):962–9.
61. Keel S, Li Z, Scheetz J, Robman L, Phung J, Makeyeva G, et al. Development and validation of a deep-learning algorithm for the detection of neovascular age-related macular degeneration from colour fundus photographs. *Clin Exp Ophthalmol*. 2019;47(8):1009–18.
62. Peng Y, Dharssi S, Chen Q, Keenan TD, Agrón E, Wong WT, et al. Deep-SeeNet: a deep learning model for automated classification of patient-based age-related macular degeneration severity from color fundus photographs. *Ophthalmology*. 2019;126(4):565–75.
63. Grassmann F, Mengelkamp J, Brandl C, Harsch S, Zimmermann ME, Linkohr B, et al. A deep learning algorithm for prediction of age-related eye disease study severity scale for age-related macular degeneration from color fundus photography. *Ophthalmology*. 2018;125(9):1410–20.
64. Liu H, Li L, Wormstone IM, Qiao C, Zhang C, Liu P, et al. Development and validation of a deep learning system to detect glaucomatous optic neuropathy using fundus photographs. *JAMA Ophthalmol*. 2019;137(12):1353–60.
65. Li Z, He Y, Keel S, Meng W, Chang RT, He M. Efficacy of a deep learning system for detecting glaucomatous optic neuropathy based on color fundus photographs. *Ophthalmology*. 2018;125(8):1199–206.
66. Marengo M, Rissotto F, Palamini A, Cutolo CA, Agosto G, Ferreras A, et al. Macular choroidal thickness: evaluation of variability among measurements and assessment of predictive value of glaucomatous visual field damage. *Ophthalmic Res*. 2022;65(4):417–24.
67. Kang SH, Hong SW, Im SK, Lee SH, Ahn MD. Effect of myopia on the thickness of the retinal nerve fiber layer measured by Cirrus HD optical coherence tomography. *Invest Ophthalmol Vis Sci*. 2010;51(8):4075–83.
68. Savini G, Barboni P, Parisi V, Carbonelli M. The influence of axial length on retinal nerve fibre layer thickness and optic-disc size measurements by spectral-domain OCT. *Br J Ophthalmol*. 2012;96(1):57–61.